Thermodynamics of Deformation of Latex Blend Coatings and Its Implications for Tailoring Their Properties

N. Agarwal* and R.J. Farris—University of Massachusetts, Amherst†

Acrylic-based latex blend coatings, comprising a hard (T_g = 45°C) and soft (T_g = –5°C) phases are evaluated in terms of the total energy they absorb before failure in a tensile test. Simultaneous measurement of the work and heat of deformation using a novel technique of differential gas pressure stretch calorimetry enables an estimate of change in their internal energy by application of the first law of thermodynamics. As the hard phase content of the blend is increased from 0-100%, its stiffness and tenacity increase, while the toughness (i.e., the energy to failure) undergoes a maximum at an intermediate composition. A partitioning of the mechanical work into heat and internal energy over the complete range of blend composition highlights the result that a simultaneous maximization of the heat dissipation and energy absorption is necessary to maximize blend toughness. This provides a new framework in which the properties of blend systems can be tailored in terms of their stiffness and toughness to design improved coatings.

INTRODUCTION

Environmental regulations have forced the paint and coatings industry to limit the emission of organic volatiles from their products during manufacturing, processing, and end use. Consequently, there is a significant focus, among the researchers in academia and industry, on developing water-based polymer coatings with zero volatile organic content (VOC). Among the areas investigated intensely are the mechanism of film formation from latexes, coalescence of polymer particles leading to interdiffusion across particle boundaries, film-forming ability of different materials, mechanical and viscoelastic properties, and blend morphology. A good collection of articles covering these areas of research is presented in a recent symposium series from the American Chemical Society.[1]

The design of protective coatings is usually based on their corrosion resistance, permeabilities, appearance, ultraviolet and chemical resistance, long-term stability, etc. The issues of stresses in multilayer coatings (leading to cracking and delamination), mechanical strength, and toughness are seldom addressed in as much detail. In this article, we present a thermodynamic evaluation of the mechanical response of a waterborne blend coatings system in terms of the work, heat, and internal energy of its deformation using the technique of differential gas pressure calorimetry developed earlier in our research group. The power of deformation calorimetry lies in the simultaneous measurement of both the heat and work of mechanical deformation. The change in internal energy of the material is then calculated using the first law of thermodynamics. Estimation of the change in internal energy is critical for a fundamental understanding of the material's response to deformation. Even though different materials, such as metals, elastomers, and glassy polymers, may show similar stress-strain curves, the underlying mechanisms controlling their deformation are quite different. Lyon,[2] for example, has shown that elastomers exhibit entropy elasticity and release heat upon stretching. Also, the hysteresis in the work expended in a closed load-unload cycle is balanced by that

Third Place Winner 1998 Roon Awards Competition. Presented at 1998 Annual Meeting of the Federation of Societies for Coatings Technology, on October 15, 1998, in New Orleans, LA.

*Current address: Corporate New Business and Technology, Kimberly-Clark Corp., 1400 Holcomb Bridge Rd., Roswell, GA 30076-2199, nagarwal@kcc.com.

†Corresponding author: Polymer Science and Engineering Dept., Silvio O. Conte National Center for Polymer Research, Amherst, MA 01003. Phone: (413) 577-3125; Fax: (413) 545-0082; email: rjfarris@polysci.umass.edu.

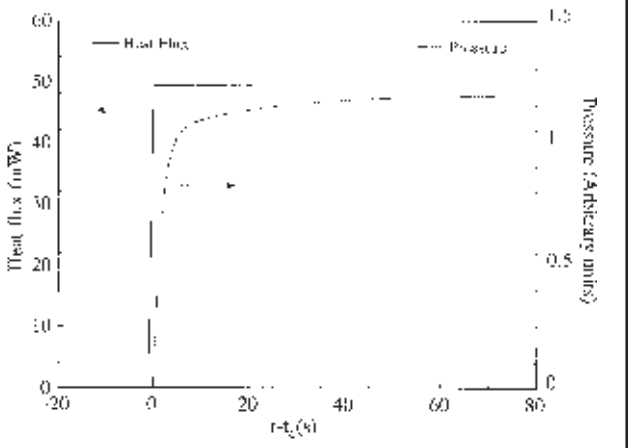

Figure 1—Theoretical differential pressure response for a constant step heating rate input.

in the heat, thereby resulting in an unchanged internal energy. When stretched to large extension ratios, these elastomers release a significant amount of heat by strain-induced crystallization which is absorbed back upon unloading. Calorimetric measurements of Adams[3,4] show that both metals and glassy polymers exhibit similar behavior in the elastic range with an endothermic response to applied tension. At large strains, however, their behavior is quite different. Most metals dissipate nearly all the applied work as heat with no change in their internal energy. Consequently, it is possible to deform them to large extensions without failure. Glassy polymers, on the other hand, are able to dissipate only a fraction (typically 40-50%) of the applied work so that their internal energy rises significantly during mechanical deformation. As a result, these polymers cannot be stretched to large extensions as mechanical failure occurs once their internal energy reaches a critical level. Adams[4] has shown that the absorbed energy remains latent in the material and is released when it is exposed to a temperature higher than the glass transition.

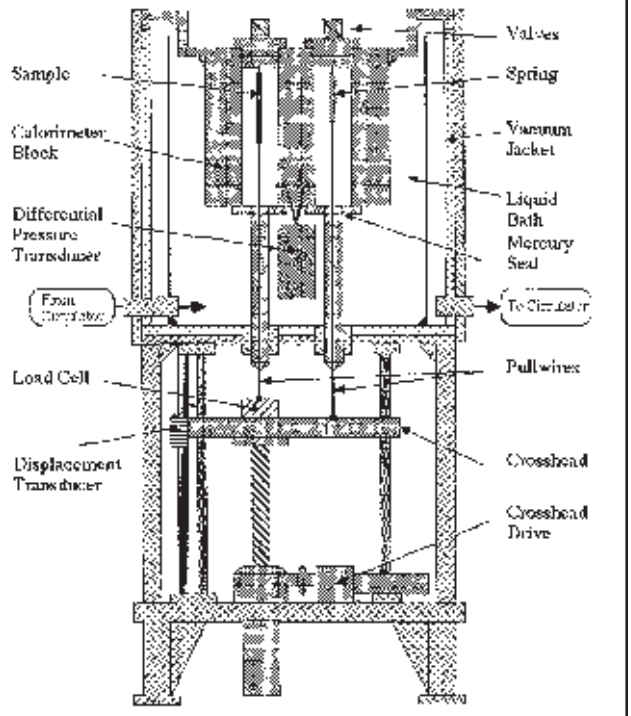

Figure 2—Schematic sketch of the deformation calorimeter.

In a multilayer coatings application, variations of temperature and humidity during end use subject the materials to cycles of stress. In each cycle, the material absorbs a fraction of the mechanical energy thereby increasing its internal energy. After several such cycles, the internal energy may rise to a level that is sufficient to cause stress cracking or delamination. It is therefore important to study the mechanical behavior of these materials from an overall energy balance approach to quantify their energy-absorption and energy-dissipating characteristics. An optimum combination of these characteristics is likely to yield materials for superior coatings performance.

In this article, we have applied the technique of differential gas pressure stretch-calorimetry to study an acrylic-based latex blend system comprising a hard (T_g = 45°C) and a soft (T_g = –5°C) phase mixed in varying proportions. The partitioning of the mechanical work into heat and internal energy change is directly measured over the complete range of blend composition expressed at the % (by volume) of the hard phase.

BACKGROUND

A Brief Historical Perspective

Interest in thermal effects arising from mechanical deformation was first sparked by John Gough[5] in 1805 who reported, among other things, that a piece of rubber felt warm to the touch upon stretching. Theoretical formulations of thermoelasticity were subsequently developed by Lord Kelvin[6] in 1857, and later verified experimentally by his associate J.P. Joule[7,8] in 1859. Nearly 70 years later, Quinney and Taylor[9,10] made more precise measurements of heat capacity changes in metals that had been cold worked in their two-step anisothermal microcalorimeter.

Duvdevani et al.[11,12] constructed the first modern deformation calorimeter based on gas thermometry to measure heats of deformation. Later, Calvet and Pratt[13] employed a pile of thermocouples in their microcalorimeter to directly measure changes in gas temperature flowing around a sample being deformed, with respect to an identical reference chamber. Their calorimeter operated on the basis of the Tian-Calvet equation,[13] which enables the calculation of heat by deconvolution of temperature-time data. Godovsky[14] later developed a completely automated version of the Calvet-Pratt calorimeter with a sensitivity down to 0.2 μW.

Muller and Engelter[15] developed the first gas pressure calorimeter that used a compensating scheme to balance the rise in differential pressure of a sealed vol-

ume of a gas in the sample chamber by providing an equal electrical heat input to the reference chamber. Lyon and Farris[2,16,17] constructed a modified version that could measure exothermic as well as endothermic heat changes upon isothermal deformation. They showed that the mathematical treatment required to yield the dynamic heat changes from pressure-time data was similar to the Tian-Calvet analysis of the temperature-time data. Lyon[18] later built another improved and more sensitive calorimeter which is used in the current research.

Stretch-calorimetric studies reported in the literature thus far have included measurements on natural rubber,[2,19-22] segmented polyurethanes,[23-28] thermoplastic homopolymers, and glassy polymers.[3,29-31] Another unique application of stretch calorimetry has been to demonstrate the gross over-estimation of strength of adhesion measured by peel testing.[32-34] It has been shown that more than 90% of the work of peel testing is either dissipated as heat or stored as latent energy of deformation via bulk deformation of the material being peeled. The peel test, consequently, provides greatly overestimated values for adhesion.

Theory of Operation

The deformation calorimeter used to measure the thermodynamics of deformation of latex blend films operates on the principle of gas pressure calorimetry. In a quasi-isothermal system, pressure changes, $\Delta P(t)$, in a fixed volume of gas surrounding the source of heat (such as a material being deformed) with respect to an identical reference chamber are related to the heat flux[2,16]:

$$\Delta P(t) = \int_0^t K(t-\xi)\frac{\partial Q(\xi)}{\partial \xi}d\xi \quad (1)$$

Where K(t) is a kernel function that is independent of sample and test conditions. Experimental data has shown that a finite sum (typically one or two terms) of exponentials can provide an excellent description of the transient response[35]:

$$K(t) = \frac{1}{C_1\tau_1}e^{-t/\tau_1} + \frac{1}{C_2\tau_2}e^{-t/\tau_2} \quad (2)$$

Where C_i and τ_i are the thermal capacitances and time constants respectively. For a constant heating rate $\dot{Q}_0$, and using the kernel function of equation (2), equation (1) yields:

$$\Delta P(t) = \dot{Q}_0\left[\frac{1}{C_1}(1-e^{-t/\tau_1}) + \frac{1}{C_2}(1-e^{-t/\tau_2})\right] \quad (3)$$

which, for long times reduces to:

$$\Delta P(\infty) = \dot{Q}_0\left(\frac{1}{C_1} + \frac{1}{C_1}\right) \quad (4)$$

Figure 1 shows a typical differential pressure response to a constant step heating rate input. Once the thermal capacitances, C_i, and time constants, τ_i, are known, equation (1) is easily deconvoluted using Laplace transforms to obtain the following relationships for dynamic heat flux and total heat[36]:

$$\dot{Q}(t) = (\alpha+\beta)\Delta P(t) + \beta\Delta\dot{P}(t) - \frac{\gamma}{\tau^*}\int_0^t \Delta P(\xi)e^{-(t-\xi)/\tau^*}d\xi \quad (5)$$

$$Q(t) = \alpha\int_0^t \Delta P(\xi)d\xi + \beta\Delta P(t) + \gamma\int_0^t \Delta P(\xi)e^{-(t-\xi)/\tau^*}d\xi \quad (6)$$

where α, β, γ, and τ^* are constants given by the following:

$$\alpha = \frac{C_1C_2}{C_1+C_2} \quad (7)$$

$$\beta = \frac{C_1C_2\tau_1\tau_2}{C_1\tau_1+C_2\tau_2} \quad (8)$$

$$\gamma = \frac{C_1C_2(\tau_1+\tau_2)}{C_1\tau_1+C_2\tau_2} - \frac{C_1C_2\tau_1\tau_2(C_1+C_2)}{(C_1\tau_1+C_2\tau_2)^2} - \frac{C_1C_2}{C_1+C_2} \quad (9)$$

$$\tau^* = \frac{C_1\tau_1+C_2\tau_2}{C_1C_2} \quad (10)$$

The total work done on the sample is available from the area under the force-displacement curve, which for constant velocity, υ_o, is given as:

$$W(t) = \upsilon_0\int_0^t f(t)dt \quad (11)$$

The change in internal energy is then estimated from equations (6) and (12) as:

$$\Delta U(t) = Q(t) + W(t) \quad (12)$$

The signs of Q(t) and W(t) are determined by whether energy is being added to the sample, or removed from it. Thus, Q(t) is negative for heat lost to surroundings (exothermic), whereas work is positive for work done on the sample.

Calorimeter Schematic

Figure 2 shows the schematic of the deformation calorimeter. The calorimeter cell block, made out of stainless steel, sits submerged in a temperature controlled bath. The cell block has two identical cylindrical cavities connected by a very sensitive differential pressure transducer. The cavities are isolated from the surroundings by values at the top and by mercury seals at the bottom. Small thin film samples are installed in the sample cavity using an Invar pullwire that exits the bottom of the cell through the airtight and frictionless mercury seal. An identical wire, connected with an elastic spring, is placed inside the reference cavity. Both of these wires are then attached to a crosshead driven by a motorized screw drive. Simultaneous movement of the two wires compensates for changes in volume of the enclosed air as the wires are pulled out of the sample and reference cavities. Pressure changes due to the dilatation of the sample are negligible in comparison to the total volume of the enclosed air in the cavity. Thin (~100 µm) polyimide baffles are installed at regular intervals in the sample cavity to minimize convection effects arising at high

Table 1—Calibration Constants Calculated from Electrical Calibration Experiments

Calibration Parameter	Value
Thermal capacitance (mW/V), C_1	10.49
Thermal capacitance (mW/V), C_2	22.59
Time constant (sec), τ_1	2.50
Time constant (sec), τ_2	44.1
Combined capacitance (mW/V), α	7.172

heating rates. Samples are deformed in a uniaxial tensile mode by pulling the support wires using a constant speed motorized screw drive. Strain rates are controlled by changing the pre-set speed of a Motomatic® motor. A Tavis model P8 transducer (0.02 psid for full scale deflection of 5V) measures the differential pressure; a Sony® GS-30E magnescale (effective length = 300 mm) measures the displacement and a 10 lb Interface® load cell measures the force on the sample. The pressure-time and the force-displacement data are thus simultaneously obtained in a single experiment.

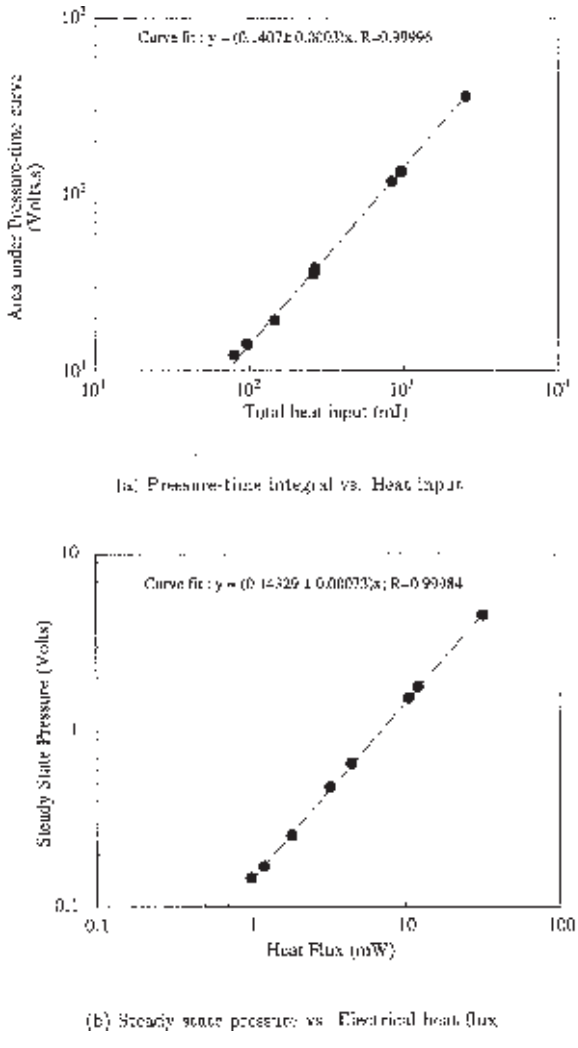

Figure 3—Pressure time integral and steady-state pressure data from electrical calibration experiments.

Calibrations

Electrical Calibrations: Thermal capacitances, C_i, and time constants, τ_i, are obtained by fitting a two-term exponential function to the response measured in a controlled calibration experiment using electrically generated heat pulses. A test wire of known resistance, supported by polyester clad copper conductors, is placed in the sample cell and a current pulse of preset magnitude and duration is passed through it in a simple electrical circuit. Steady-state pressure-time response for long pulses of duration much greater than the system time constants yields the required thermal capacitances and time constants. The area under the pressure-time curve, long after the pulse is over, is also linearly related to the total heat input; the constant of proportionality being a measure of the total thermal capacitance of the combined sample instrument system.

Figures 3a and b show the data used to determine the calibration constant in a typical calibration experiment with a 10 cm long nichrome wire having a resistance of 12.79 Ω and pulse magnitudes of 8-50 mA and durations of 80 sec. The slope of a linear regression, forced through the origin, of the pressure-time integral versus total heat, and steady-state pressure versus pulse magnitude yields the inverse of the overall calibration constant α given by equation (7). The thermal capacitances and time constants for the sample and the calorimeter are calculated by the best fit of the pressure-time data, and the results are shown in *Table* 1.

It is seen from the calibration data that the linearity of the pressure response to the input heat flux is maintained over several decades of the input values. Effects of the change in length of the sample, as it is stretched in an actual experiment, on the calibration constant are simulated using wires of varying lengths. Again, as shown in *Figures* 4a and b, the calibration constant is not affected by the length of the heating source.

Calibrations with Natural Rubber: In order to get a complete energy balance, and values of changes in internal energy from equation (13), we need to ensure that both heat and work values are correct. This is accomplished by measuring the heat and work of deformation of an elastic material such as natural rubber. A rubber band, in the shape of a loop, supported by the Invar pullwires, is placed inside the sample cell of the calorimeter and stretched to various extension ratios and subsequently unloaded back to the original length. Since the overall change in internal energy over the complete load-unload cycle is zero for a reversible process, the hysteresis in work should match exactly that in the heat.

Typical profiles of the differential pressure and the force in response to the stretching of the rubber band is shown in *Figure* 5 as a function of the extension ratio. Initially, there is a small exothermic trend, almost at a constant rate, due to the loss of entropy of the material. At around an extension ratio of four, there is a sharp rise in pressure indicating the onset of strain-induced crystallization. Upon holding the sample at the extension ratio of five, the pressure gradually returns to the baseline value, while the force relaxes to a stable value. Upon subsequent unloading, there is a protracted endotherm in pressure indicating the melting of crystals, which is

followed by a gradual rise to the original baseline pressure at zero stretch. As explained by Lyon,[2] there is a combination of crystal melting and recrystallization during the unloading of rubber.

Figure 6 displays the calculated heat, work, and internal energy profiles normalized by the weight of the sample, as a function of the extension ratio. As shown, the overall change in internal energy over the cycle is nearly zero. During the loading half, the internal energy reduces by around –5 J/g due to strain-induced crystallization.

EXPERIMENTAL

Materials and Sample Preparation

Methylmethacrylate-based copolymer latexes were synthesized by Dr. G.D. Andrews of the DuPont Company. The first latex was poly(methyl methacrylate-co-ethyl acrylate), P(MMA-co-EA), with a T_g of 45°C, and the second poly(methyl methacrylate-co-butyl acrylate), P(MMA-co-BA), with a T_g of –5°C. The co-monomer molar ratios in the two latexes were 3:2 and 2:3, respectively, and these were stabilized by 0.35 and 0.17% (on molar basis) ammonium lauryl sulfate (ALS). Particle sizes of these latexes, as measured by dynamic light scattering, were of the order of 100 nm. Unless mentioned otherwise, these two copolymers will be referred to as "hard" and "soft" in the subsequent description.

Blend films of the two copolymers were cast from the aqueous dispersions on a glass plate, dried at 70°C for 3-4 hr and annealed at 130°C for 20 min. Films were easily removed from the glass plates with the aid of water. The time of exposure to water was minimized so as to limit the amount of absorbed water, and excess water was wiped off from the surface with Kimwipes®. The films

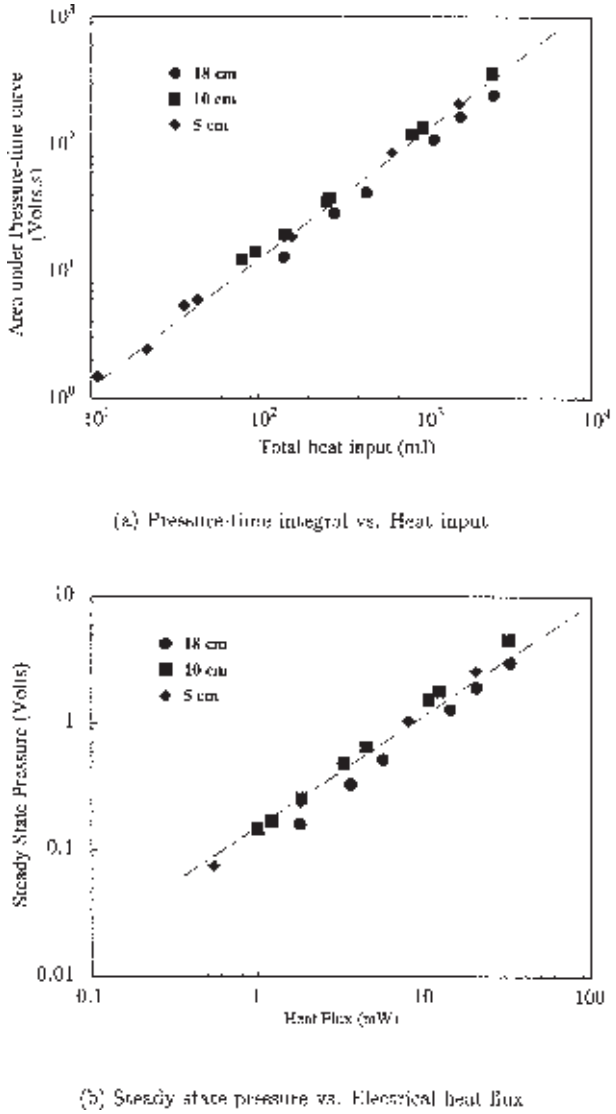

Figure 4—Pressure time integral and steady-state pressure data from electrical calibration experiments as a function of source lengths.

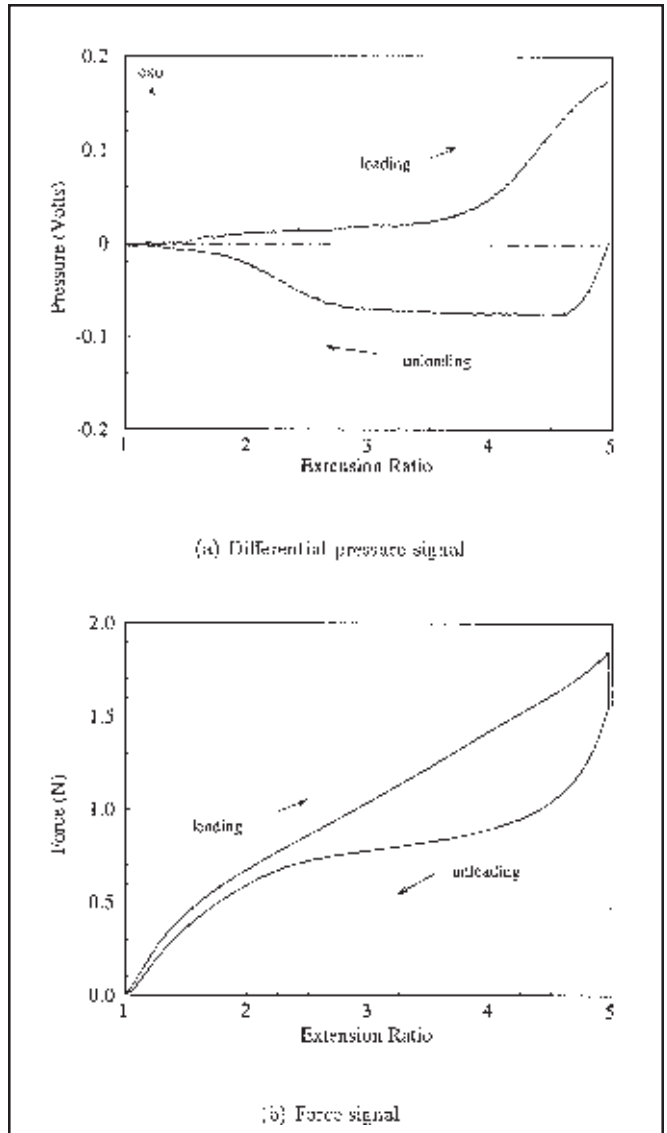

Figure 5—Differential pressure and force vs. extension ratio for loading and unloading of natural rubber.

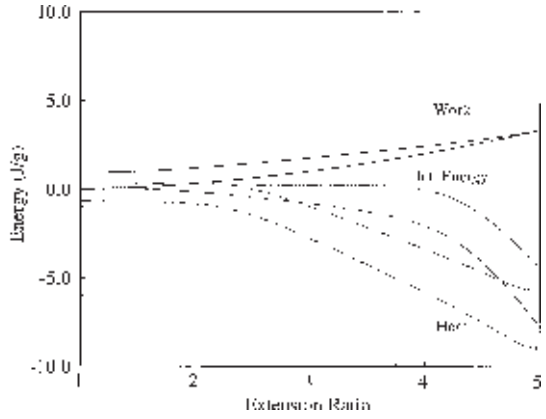

Figure 6—Heat, work, and internal energy of deformation of rubber in the calorimeter at 25°C.

were later left to dry at room conditions. The composition of the blends was varied from 0% hard to 100% hard phase to obtain a complete set.

It was further necessary to hot press these samples at 130°C to get uniformly thick films for mechanical testing. The resulting thickness ranged between 100-200 µm, and the films were annealed for a week at 50°C to remove any thermal history. All of the blend films were clear and transparent although the hardness and dimensional stability varied from very soft to hard with the concentration of the hard phase. The soft blends (20% or lower hard phase) were extremely tacky, and it was necessary to apply a thin coat of talcum powder to prevent adhesion to work surfaces. ASTM D 638 (Type V) dog-bone shaped samples were cut out of these films for subsequent testing.

Techniques

Tensile Testing: Tensile testing was carried out using an Instron™ model 5564 at room temperature. The data was collected and analyzed using the Merlin Series IX software. Samples were stretched with a crosshead speed of 8.58 mm/min that corresponded to a strain-rate of 0.9/min for a gauge length of 9.53 mm. An optical extensometer, connected via a video camera, was used to measure the displacement in the first one percent strain of the sample for accurate estimation of the Young's moduli.

Modulated Differential Scanning Calorimetry: Modulated differential scanning calorimetry (MDSC) experiments were carried out using a DSC2910 module from TA Instruments under a helium (He) purge at a flowrate of 80 ml/min. Small pieces (20-30 mg) were cut from dried blend films and encapsulated in hermetically sealed aluminum pans. The weights of the sample and reference pans were matched to within 0.5 mg. Calibrations for cell constant and specific heat relied on indium and sapphire standards, respectively. Each experiment involved cooling the sample from 90°C to –40°C at 2°C / min with a temperature amplitude of ± 0.5°C and a period of oscillation of 40s. Glass transition temperatures were estimated by the half-width method.

Stretch Calorimetry: Dog-bone shaped samples (ASTM D 638, Type V) were mounted inside the calorimeter cell using the method described by Adams,[3] and were left to equilibrate at 25°C for at least five hours. After equilibration, they were stretched at a strain rate of 0.9/min to an extension ratio close to their break point determined earlier by Instron. The soft samples (0-30% hard phase) could be loaded only to an extension ratio of 8.4, which is much lower than their ultimate break point, due to the limitation on the total displacement of the crosshead in the calorimeter. Once the force and pressure signals stabilized at this extension, they were unloaded back to zero load. The energy values were calculated over the entire load-unload cycle and normalized by the weight of the sample between the grips. Similar experiments were conducted at 60°C; a temperature above the T_g of the two phases. The strain rate in this case was approximately 1.9/min, as the corresponding value of 0.9/min used in experiments at 25°C yielded poor signal-to-noise ratio in the calorimeter signal.

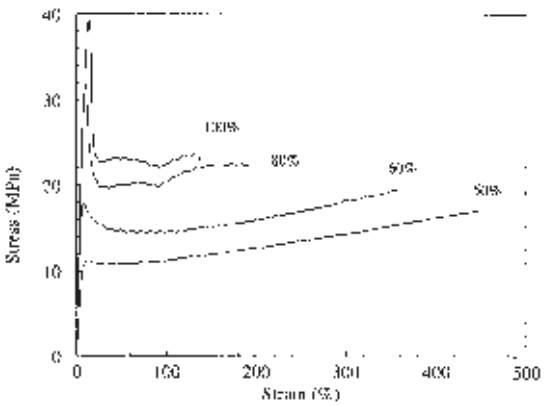

(a) Blends with 50% and more hard phase

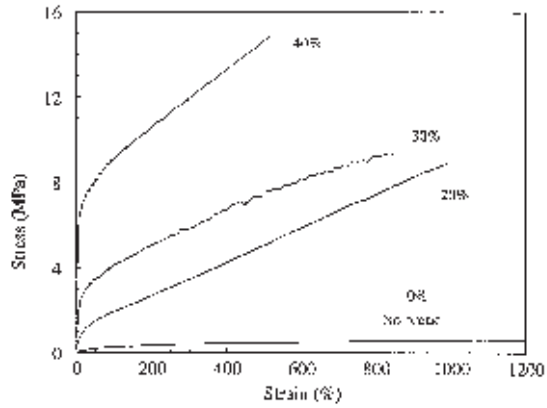

(b) Blends with less than 50% hard phase

Figure 7—Stress-strain curves for acrylic blends. Percent numbers indicate volume % hard phase.

RESULTS AND DISCUSSION

Thermo-Mechanical Characterization

The stress-strain curves for hard blends (with 50% or more of the hard phase) and the soft blends (with less than 50% of the hard phase) are presented in *Figure* 7. The soft blends are rubber-like and stretch to large ultimate strains; the pure soft phase does not break even at 2500%. The hard blends, on the other hand, show distinct yield points and fail at lower strains. Although a yield point is seen for blends with 50 and 60% hard content, there is no neck formation. Blends with 80% hard phase, and the pure hard phase, form stable necks that grow beyond their respective yield points. The hard blends show extensive stress whitening that disappears on heating above 50°C. The soft blends show stress whitening when they are stretched to large extensions but return to their initial clear state after failure. This observation of whitening upon stretching is typical of two-phase systems comprising of hard and soft components, and has been ascribed to crazing of the glassy matrix or cavitation of the rubbery particles.

Figure 8 shows the experimentally observed values of Young's moduli obtained from an Instron. These values lie within the Hashin-Shtrikman bounds[37,38] and are in close agreement with the solution of Hill-Budiansky equations.[39,40] Similar results on systems of hard and soft phases have been interpreted within the framework of a percolation concept by Hsu[41,42] and his co-workers. During their study on block copolymers of styrene and butadiene,[41] and blends of a thermoplastic polyester with ethylene-propylene-diene (EPDM) rubber,[42] they found that there was a rubber-to-glass transition upon increasing the concentration of the hard phase (polystyrene and polyester respectively in the previous references). At low concentrations of the hard phase, they argue, the mechanical response of the composite system is controlled by the continuous soft matrix, as the particles of the hard phase cannot interact with one another. On the other extreme, the continuous hard phase controls the overall response. A transition region must, therefore, occur at an intermediate composition when the regions of hard phase just begin to interact in a cooperative manner. This composition is called the percolation threshold; an idea first introduced for elastic networks by De Gennes[43] based on an approach similar to that adopted for conductivity of a random network of resistors. The moduli of our samples show that such a transition occurs in the range of 20-40% hard phase in the blend.

The glass transition temperatures for the hard and soft phases in the blends were calculated from MDSC by the mid-point method and are shown in *Figure* 9. The T_g of the hard phase is not affected by the composition of the blend, whereas that of the soft phase shows a small depression upon increasing the concentration of the hard phase in the blend. A mismatch in thermal expansion coefficients between the hard and soft phases introduces an interfacial pressure as the blend is cooled from above the T_g. Using the pressure dependence of T_g for poly(methyl methacrylate) as a first approximation, Agarwal et al.[44] estimated a depression of 3-10°C in the T_g of the soft phase. Similar results have been observed for blends of polystyrenes with rubber, such as acrylonitrile-butadiene-styrene (ABS), in which the T_g of the soft component (butadiene) is lowered by as much as 10°C due to the presence of the hard phase. A complete thermal characterization of these acrylic blends is presented elsewhere.[45]

Stretch-Calorimetry

Properties of the Pure Components: The pressure versus extension ratio profiles shown in *Figures* 10a and b highlight the different nature of the hard and soft pure components. The pressure values have been normalized by the sample weight for a paper comparison, and are directly related to the transducer voltage (full scale deflection of 5V corresponds to a differential pressure of 0.02 psid). The deformation of the soft phase is almost entirely entropic, as the pressure rise upon stretching indicates an exothermic response to the input energy. Upon unloading, the sample recovers part of the lost entropy during stretching as shown by the corresponding endothermic pressure change.

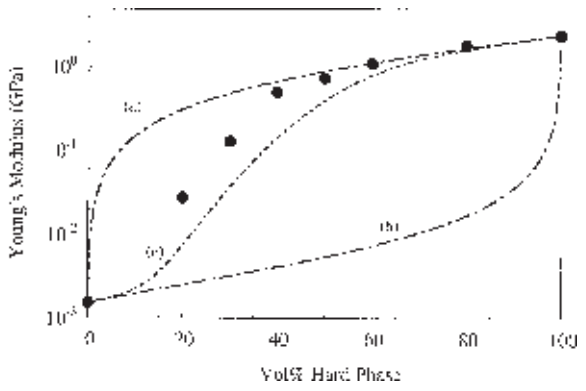

Figure 8—Young's moduli for blends as a function of composition. (a) and (b) Hashin-Shtrikman bounds; (c) Hill-Budiansky theory.

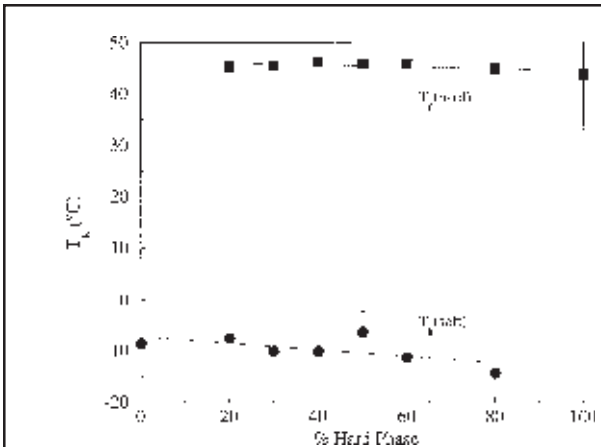

Figure 9—Glass transition temperatures of the hard and soft phases for blends.

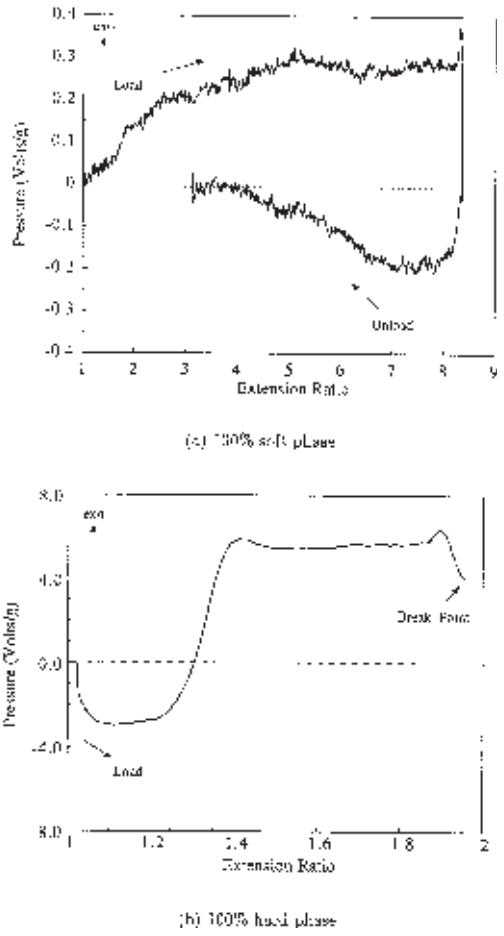

Figure 10—Differential pressure change of the pure soft and hard phases in the calorimeter at 25°C at a strain-rate of 0.9/min.

The pure hard phase, on the other hand, responds to the imposed deformation in a typical glassy solid-like manner as the differential pressure profile shows an initial endothermic trend. This is easily explained by equations of linear thermoelasticity[2] that predict an endothermic response for a material with a positive expansion coefficient. Once the sample yields, the differential pressure is exothermic due to energy dissipation during the plastic deformation.

The calculated profiles of the work, heat, and internal energy for the pure soft phase, as shown in *Figure* 11, further highlights the entropic nature of its elasticity. As the material is stretched, the input work is almost entirely converted into heat on account of a loss of entropy as well as viscous dissipation; the change in internal energy being slightly negative during the process. Upon unloading, a part of the work of loading is recovered following a corresponding increase in entropy. A large residual strain, nearly twice the original length, still remains in the sample at the end of the cycle as a result of inelastic deformation, which mostly corresponds to viscous flow as it does not show any significant increase in the overall internal energy of the material.

The endothermic heat response of the pure hard phase, indicating its energy elasticity, is clearly seen in the calculated profiles of the work, heat, and internal energy shown in *Figure* 12. The internal energy of the material increases more than the input work owing to an additional heat absorption from the surroundings arising from the thermoelastic effect. During the plastic deformation beyond the yield point, the rise in internal energy is reduced by increased heat dissipation. These energy values correspond only to the stretching of the material since the sample failed during the stabilization period at the end of loading. However, these values are not expected to be much in error even if the unloading half of the normal load-unload cycle could be included. The recoverable work of unloading after large plastic deformations is typically quite insignificant in comparison to the overall work of loading for such glassy polymers. A small exotherm is expected in heat upon unloading due to the thermoelastic effects; its magnitude, however, is likely to be much smaller than the heat dissipation during plastic deformation.

In contrast to the pure soft phase, the pure hard phase absorbs a significant fraction of the input work as an increase in its internal energy. This observation is consistent with Adam's measurements on a glassy poly-

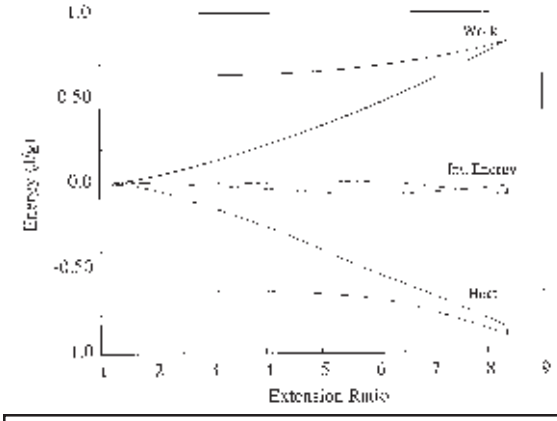

Figure 11—Work, heat, and internal energy changes for the pure soft phase in the calorimeter at 25°C.

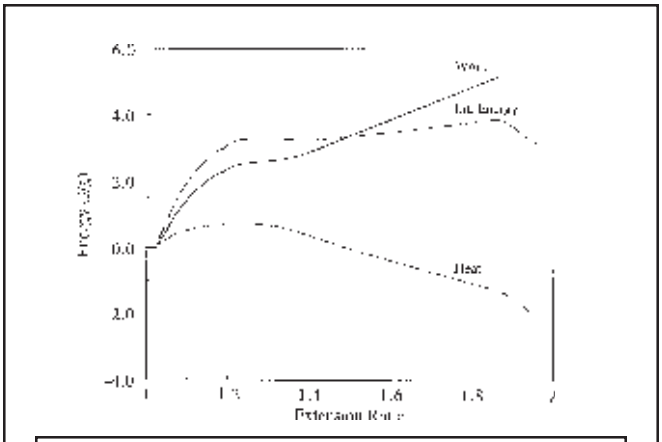

Figure 12—Work, heat, and internal energy changes for the pure hard phase in the calorimeter at 25°C.

mer[3,4] that absorb nearly 50% of the input work as additions to their internal energies. When a glassy polymer is deformed to large extensions, its constituent molecules are oriented along the stretch direction resulting in a loss of entropy. In addition, a large fraction of the input energy is stored in the stretched bonds. When the applied force is removed, these molecules are unable to relax to their original low energy state due to the glassy nature of the material. The stored energy, therefore, is analogous to a latent energy of deformation that can be released at high temperatures or by physical aging over long periods of time.

Godovsky[14] has summarized the various mechanisms by which energy could be dissipated or absorbed by polymeric materials:

(1) Strain-induced crystallization and other phase transformations.

(2) *Intra*-molecular conformation changes.

(3) Changes in the *inter*-molecular environment, such as hydrogen bonding, Van der Waals attraction, ionic interaction, etc.

(4) "Dislocations" of amorphous glasses associated with plastic deformation below their T_g.

(5) *Intra*-, as well, as *inter*-molecular friction.

(6) Creation of new surfaces in the form of crazes and cavities.

(7) Bond rupture.

The extent to which mechanisms influence the overall energy dissipation or absorption characteristics of a material is, quite naturally, dependent on its structure and morphology. In the present case, both the pure phases are completely amorphous; crystalline phase transitions are therefore ruled out. It appears that the deformation of the pure soft phase primarily results in recoverable conformational changes and viscous dissipation. The pure hard phase, on the other hand, absorbs a large fraction of the input work as latent energy of deformation.

Properties of the Blends: Blends of these hard and soft components in varying compositions were deformed in the calorimeter in a similar way, the results of which are shown in *Figures* 13-15. Again, the ultimate extension ratio was close to the break point determined earlier by Instron. Energy values, normalized by the sample weight, are calculated for the entire load-unload cycle.

The work of loading, as shown in *Figure* 13, increases with the extent of deformation and reaches a maximum for the final extension ratio of loading in each case. Upon unloading, part of the work, corresponding to reversible bond conformations, is recovered although the absolute values are much smaller than that expended during loading. The degree to which the expended work is recoverable during unloading diminishes severely for the hard blends (hard phase content of 30% or more) as indicated by progressively large relative residual strains at the end of the load-unload cycle. The predominantly glassy nature of these hard blends prevents the recovery of the conformational changes occurring upon deformation.

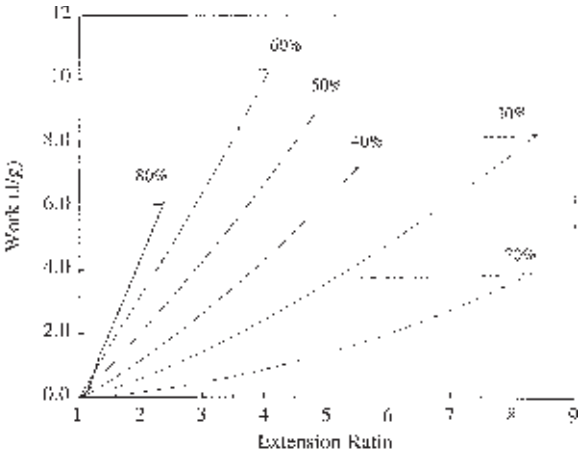

Figure 13—Work of cyclic deformation for blends at 25°C. Percent numbers indicate volume % hard phase.

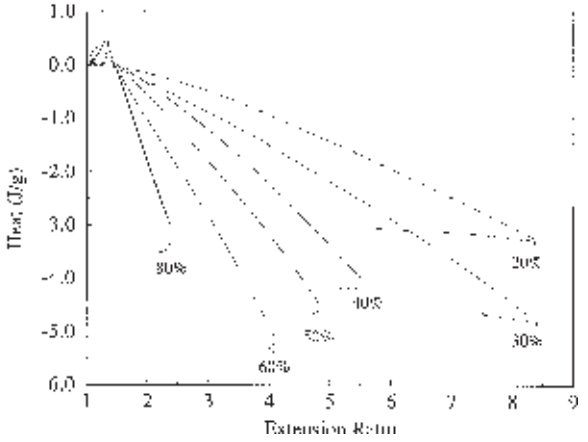

Figure 14—Heat of cyclic deformation for blends at 25°C. Percent numbers indicate volume % hard phase.

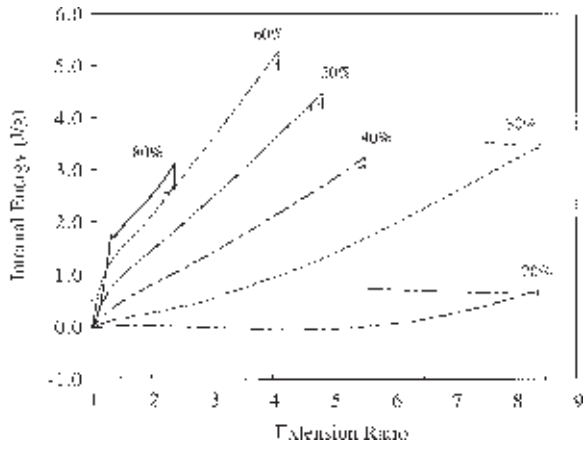

Figure 15—Change in internal energy of cyclic deformation for blends at 25°C. Percent numbers indicate volume % hard phase.

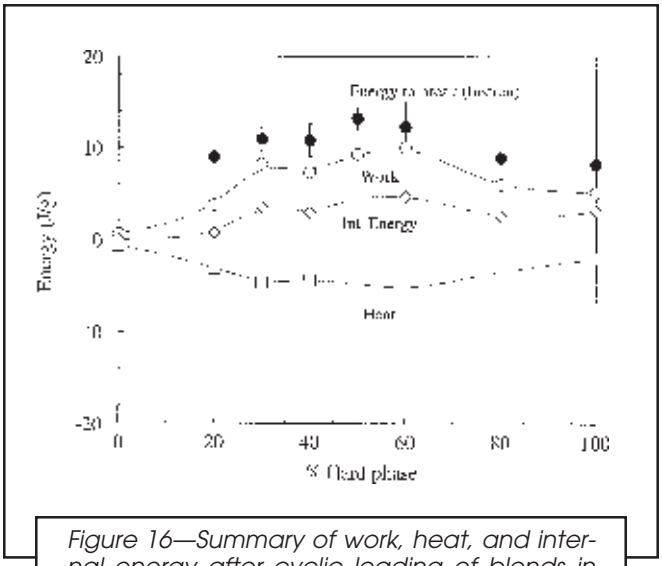

Figure 16—Summary of work, heat, and internal energy after cyclic loading of blends in the calorimeter at 25°C. Filled circles show the energy to break values obtained from Instron.

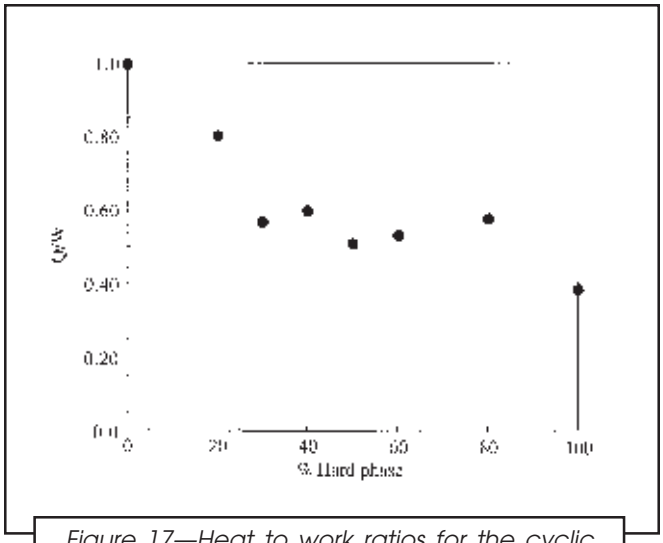

Figure 17—Heat to work ratios for the cyclic deformation of blends in the calorimeter at 25°C.

Figure 14 shows an interesting pattern in the heat profiles for these blends. Although all of the blends exhibit a larger part of the work being dissipated as heat of plastic deformation, the heat profiles below an extension ratio of 1.5 are remarkably different for the hard and soft blends. These differences arise from the endothermic elastic response of the hard blends before the yield point owing to their positive thermal expansion coefficients. The magnitude of the endotherm is directly proportional to the Young's modulus; higher concentrations of the hard phase in the blends, consequently, result in a stronger endotherm. The soft blends, on the other hand, behave more or less like a rubber, showing an exothermic heat profile all throughout their deformation.

The change in internal energy of these blends, as a function of extension ratio, is shown in *Figure* 15. There is a significant increase in the internal energy at the end of a load-unload cycle for the hard blends. At a small extension ratio, such as 2.0, the change in internal energy is proportional to the blend stiffness; the largest increase being shown by the blend with 80% hard phase which has a modulus of 1.8 GPa compared with that of 2.7 MPa for the 20% hard blend. Even at large extension ratios, where the range of blends available for comparison is smaller, the stiffer blends have a higher level of internal energy.

Figures 13-15 show that the transformation to soft rubber-like behavior with large heat dissipation and small increase in internal energy, to hard glass-like behavior with larger internal energy increases, occurs around 30% hard phase in the blend. This composition is in excellent agreement with the mechanical and morphological data that has been interpreted within the framework of a percolation theory.[44] Blends with hard phase contents ranging between 30-40%, undergo a transition from a soft continuous matrix with hard dispersions, to a hard continuous matrix with soft dispersions. This phase inversion affects the manner in which energy is dissipated or stored by the blend; the dominance of one over the other being governed by the stiffness of the continuous phase.

Figure 16 summarizes the values of work, heat, and internal energy for all the blends as a function of their hard phase content at the end of a load-unload cycle. Also shown are the energy to break values (represented by filled circles) measured by Instron. The work values from the calorimeter are lower as the samples were stretched to extension ratios lower than their breakpoints; however, their trend is similar to that measured by Instron. Both energy dissipation and energy absorption increase as the concentration of the hard phase is increased in the blend and a maximum is seen at 50-60% hard phase.

Below the composition of matrix phase inversion (~30% hard phase), a larger fraction of the work is dissi-

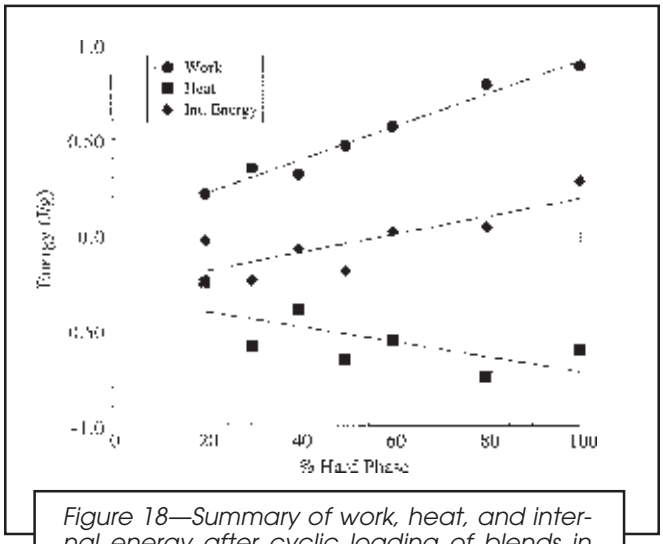

Figure 18—Summary of work, heat, and internal energy after cyclic loading of blends in the calorimeter stretched at 60°C with a strain rate of 1.9/min.

pated as heat as shown by the heat to work ratio (Q/W) values in *Figure* 17. Blends with a higher proportion of the pure hard phase exhibit relatively constant Q/W within 0.5-0.6. The value for the pure hard phase is lower at approximately 0.4; however, it has a relatively high degree of uncertainty arising from sample fracture. The invariance in Q/W implies that the ratio of internal energy to work (ΔU/W) is also invariant within the uncertainty of measurement. The rising values of work for blends having 30-60% hard phase, then, result in a greater rise in the internal energy. The maximum in work for blends with 50-60% hard phase is, therefore, due to a simultaneous maximization of energy dissipation and energy absorption.

Upon increasing the hard phase content of the blend beyond 60%, there is a reduction in both work and heat values due to a decrease in the extensibility. Although higher stiffness values for these blends enable them to support a higher force, a sharp decrease in the elongation to break results in lower values for the work (i.e., the area under the force-displacement curve). The observed decreasing trend in the internal energy change is supported by the invariance of Q/W values shown in *Figure* 17. These results clearly demonstrate a synergistic behavior of both the blend components to yield an optimum combination of stiffness and toughness for the 60% hard blend.

At 60°C, both of the blend components are above their T_g, although their moduli still differ by an order of magnitude.[44] However, there is little difference between their energy absorption and dissipation characteristics, as both are rubbery materials above the glass transition temperature. *Figure* 18 summarizes the values of work, heat, and internal energy at the end of a complete load-unload cycle for a maximum extension ratio of 8.4. The two-phase, rubber and glass-like response seen in *Figure* 16, is absent at 60°C, and the variation in the work of deformation is entirely due to the differences in blend stiffness. A linear regression through the work, heat, and energy data indicates that a simple rule of mixtures adequately describes the energy behavior of these blends.

At low hard content, the soft blends dissipate almost 100% of the input work as heat with no net change in the internal energy. Negative data points for the internal energy change shown in *Figure* 18 are within the uncertainty of measurement on account of a low signal-to-noise ratio. As the concentration of the hard phase is increased, the blends show a slight increase in their internal energy; however most of the work is again dissipated as heat. The energy absorbing capability of the hard phase is still significant despite a much diminished stiffness.

In summary, our results provide ample motivation for considering an optimization of both stiffness and toughness of the coatings materials for improved performance. Using a blend of different materials, it is possible to improve film-formation characteristics, as well as obtain long-term mechanical durability by maximizing the toughness. A careful control of the Q/W ratio by manipulating the pure component properties and blend morphology provides another tool for designing durable coatings.

CONCLUSIONS

The distribution of work into heat and stored energy for acrylic latex blend films has been studied using a deformation calorimeter, at constant temperature and strain rate as a function of their hard phase content. The soft blends are rubber-like, stretch to high strains, and dissipate a larger fraction of input work as heat. The hard blends are more glassy and solid-like, and absorb a larger fraction of work as increase in their internal energy. Appearance of an initial endothermic trend at small extensions for blends with more than 30% hard phase indicates a transformation to a hard continuous matrix with soft dispersions consistent with the elastic properties measured earlier and interpreted within the framework of a percolation theory. Blends with 60% hard phase show a maximum in toughness by a simultaneous maximization of heat dissipation and energy absorption. These results provide a new framework for selecting materials for superior coatings performance by a careful consideration of the balance between energy dissipation and energy absorption in terms of the Q/W ratio.

ACKNOWLEDGMENTS

The authors acknowledge the Materials Research Science and Engineering Center (MRSEC) at the University of Massachusetts, Amherst, for use of their research facilities. Financial support was provided by the DuPont Company through the Center for University of Massachusetts Industry Research on Polymers (CUMIRP). We thank Dr. G.D. Andrews and Dr. S. Mazur of DuPont for synthesizing the latexes and helpful discussions. This work forms a part of N. Agarwal's Ph.D. dissertation and he gratefully acknowledges the contribution of Dr. Mazur on his research committee.

Nomenclature

- C_1, C_2 — Thermal Capacitance (mW/V)
- f(t) — force (N)
- K(t) — Kernel function describing the transient response of the stretch calorimeter
- Q(t) — Dynamic Heat flow measured in the stretch calorimeter (J/g)
- $\dot{Q}$ — Heat flux (mW)
- $\dot{Q}_o$ — Constant heat flux in calibration experiments (mW)
- ΔP(t) — Differential pressure measured in the stretch calorimeter (Volts)
- ΔP(∞) — Steady state differential pressure at constant heat flux (Volts)
- t — Time (s)
- ΔU(t) — Change in internal energy (J/g)
- v_0 — Velocity of sample deformation (mm/s)
- W(t) — Dynamic work calculated from force and displacement data (J/g)
- α, β, γ, δ, τ*—Calibration constants related to thermal capcitances and time constants.
- τ_1, τ_2 — Time constants (s)

References

(1) Provder, T., Winnik, M.A., and Urban, M.W. (Eds.), *ACS Symposium Series*, Volume 648, American Chemical Society, Washington, D.C., 1996.
(2) Lyon, R.E., "Thermodynamics of Deformation," Ph.D. Thesis, University of Massachusetts, Amherst, 1985.
(3) Adams, G.W., "The Thermodynamics of Deformation for Thermoplastic Polymers," Ph.D. Thesis, University of Massachusetts, Amherst, 1987.
(4) Adams, G.W. and Farris, R.J., *Polymer*, 30, 1824 (1989).
(5) Gough, J., *Proc. Lit. Phil. Soc., Manchester, 2* ser., 1,288 (1805).
(6) Lord Kelvin, *Quarterly J. Math*, 1,57 (1857).
(7) Joule, J.P., *Trans. Roy. Soc., London*, A149,91 (1859).
(8) Joule, J.P., *Phil. Mag*., 14, 227 (1857).
(9) Taylor, G.I. and Quinney, H., *Proc. Roy. Soc. London*, A 143, 307 (1934).
(10) Quinney, H. and Taylor, G.I., *Proc. Roy. Soc. London*, A 163, 157 (1937).
(11) Duvdevani, I.J., Biesenberger, J.A., and Gogos, C.G., *Polymer Eng. & Sci*., 9 (4), 250 (1969).
(12) Duvdevani, I.J., Biesenberger, J.A., and Gogos, C.G., *Polymer Eng. & Sci*., 10 (6), 320 (1979).
(13) Calvet, E. and Prat, H., *Recent Progress in Microcalorimetry*, Macmillan Co., New York, 1963.
(14) Godovsky, Y.K., *Thermophysical Properties of Polymers*, Springer-Verlag, New York, 1992.
(15) Muller, F.H. and Engelter, A., *Rheol. Acta*., 1, 39 (1958).
(16) Lyon, R.E. and Farris, R.J., *Rev. Sci. Instrum*., 57 (8), 1640 (1986).
(17) Lyon, R.E. and Farris, R.J., U.S. Patent No. 4,761,078 (1988).
(18) Lyon, R.E. and Raboin, P.J., *J. Therm. Anal*., 44, 777 (1995).
(19) Godovsky, Y.K., *Polymer*, 22, 75 (1981).
(20) Araimo, L., de Candia, F., and Vittoria, V., *Polymer*, 19, 731 (1978).
(21) Price, C., Evans, K.A., and de Candia, F., *Polymer*, 14, 338 (1973).
(22) Araimo, L., de Candia, F., and Vittoria, V., *Polymer*, 17, 731 (1976).
(23) Godovsky, Y.K., Bessonova, N.P., and Mironova, N.N., *Colloid Polymer Sci*., 264, 224 (1986).
(24) Godovsky, Y.K., Bessonova, N.P., and Mironova, N.N., *Colloid Polymer Sci*., 267, 414 (1989).
(25) Godovsky, Y.K., and Bessonova, N.P., *Colloid & Polymer Sci*., 261, 645 (1983).
(26) Dexi, W., Lyon, R.E., and Farris, R.J., *Chinese J. Polymer Sci*., 3, 262 (1987).
(27) Godovsky, Y.K., *Makromol. Chem. Suppl*., 6, 117 (1984).
(28) Godovsky, Y.K., and Bessonova, N.P., *Thermochimica Acta*, 247, 19 (1994).
(29) Godovsky, Y.K., *Colloid Polymer Sci*., 260, 461 (1982).
(30) Salamatina, O.B., Hohne, G.W.H., Rudnev, S.N., and Oleinik, E.F., *Thermochimica Acta*, 241, 1 (1994).
(31) Lyon, R.E. and Farris, R.J., *Polymer Eng. Sci*., 24 (11), 908 (1984).
(32) Goldfarb, J.L., Farris, R.J., Chai, Z., and Karasz, F.E., *Mat. Res. Soc. Symp. Proc*., 227, 335 (1991).
(33) Goldfarb, J.L. and Farris, R.J., *J. Adhesion*, 35, 233 (1991).
(34) Goldfarb, J.L., "A Calorimetric Evaluation of the Peel Adhesion Test," Ph.D. Thesis, University of Massachusetts, Amherst, 1992.
(35) Lyon, R.E. and Farris, R.J., *Thermochimica Acta*, 161, 287 (1990).
(36) Lyon, R.E. and Abramowitz, A., *Fire Mat*., 19, 11 (1995).
(37) Hashin, Z., *J. Appl. Mech*., 29, 143 (1962).
(38) Hashin, Z. and Shtrikman, S., *J. Mech. Phys. Solids*, 11, 127 (1963).
(39) Hill, R., *J. Mech. Phys. Solids*, 13, 213 (1965).
(40) Budiansky, B., *J. Mech. Phys. Solids*, 13, 223 (1965).
(41) Hsu, W.Y., Giri, M.R., and Ikeda, R.M., *Macromolecules*, 15, 1210 (1982).
(42) Hsu, W.Y. and Wu, S., *Polymer Eng. Sci*., 33 (5), 293 (1993).
(43) de Gennes, P.G., *J. de Physique-letters*, 37, L1 (1976).
(44) Agarwal, N. and Farris, R.J., *Polymer Eng. Sci*., (1998), in press.
(45) Agarwal, N. and Farris, R.J., *Thermochimica Acta*, (1998), in press.